Secondary Ion Emission from Water Ice at 10−130 K Induced by MeV N2+ Ions

ARTICLE *in* THE JOURNAL OF PHYSICAL CHEMISTRY C · MAY 2011

Impact Factor: 4.77 · DOI: 10.1021/jp111152y

THE JOURNAL OF PHYSICAL CHEMISTRY C

ARTICLE

pubs.acs.org/JPCC

Secondary Ion Emission from Water Ice at 10−130 K Induced by MeV N^{2+} Ions

A. L. F. de Barros,[*,†] L. S. Farenzena,[‡] D. P. P. Andrade,[§,⊥] E. F. da Silveira,[⊥] and K. Wien[¶]

[†]Departamento de Disciplinas Básicas e Gerais, CEFET-RJ, Rio de Janeiro, RJ, Brazil

[‡]Departamento de Física, Universidade Federal de Santa Catarina, Florianópolis, Brazil

[§]Universidade do Vale do Paraíba, São José dos Campos, SP, Brazil

[⊥]Departamento de Física, Pontifícia Universidade Católica do Rio de Janeiro, Rio de Janeiro, RJ, Brazil

[¶]Technische Universität Darmstadt, Darmstadt, Germany

ABSTRACT: Secondary ion emission from vapor-deposited water ice has been investigated in exploring the influence of phase transitions on the desorption yield of H_2O ions, particularly, the hydronium H_3O^+ and the cluster ions $(H_2O)_nH_3O^+$. For 1.5 MeV N^{2+} ion bombardment on water ice at a temperature of ∼80 K, the sum of the yields of H_3O^+ and of the cluster ions represents 80% of the positive ion yield (i.e., 0.23 ions/impact) and 0.33% of the total H_2O molecular sputtering yield. When the beam energy of N^{2+} is varied between 0.5 and 1.7 MeV, the shape of the cluster mass distributions does not change and the total cluster ion yield scales with the third power of the electronic energy loss. Time-of-flight mass spectra were taken during the warming up of the ice from 10 to 216 K. Up to 30 K, the cluster ion yields are approximately constant, whereas between 30 and 75 K, they decrease gradually by a factor 6.5 and remain constant until 130 K. This is in analogy with modifications in the ice structure: in the 38−78 K region, the amorphous ice phases change gradually from the high-density to low-density form. The high ion yields below 30 K are supposedly caused by a reduction of charge carrier transport in high-density amorphous ice. The yield ratio of $Y((H_2O)H_3O^+)/Y(H_3O^+)$, measured as a function of time/temperature, exhibits clearly the three amorphous regimes and, above 130 K, the change in the composition of the top layer of the ice due to enrichment with organic material. This procedure offers a reliable method to identify structural changes of water ice, such as phase transitions.

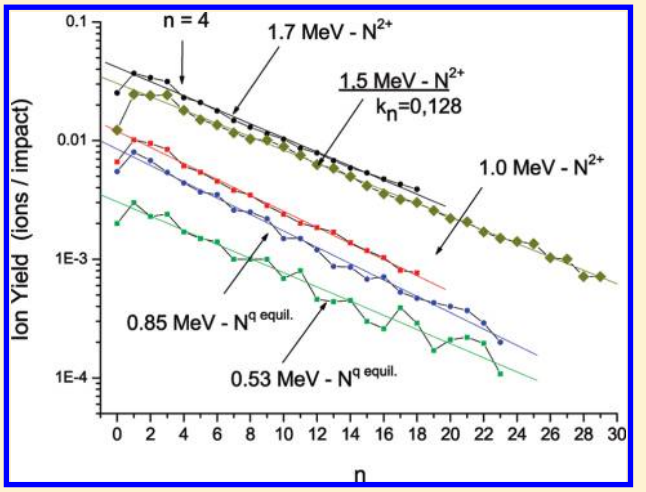

1. INTRODUCTION

The existence of many crystalline and amorphous states of solid water has been established for a long time. A review on water ice phase transitions can be found, for instance, in the book of Petrenko and Whitworth.[1] Jenniskens et al.[2] studied amorphous ice by electron diffraction at the temperature range of 15−100 K and confirmed the existence of two forms of amorphous ice, a high-density form (I_{ah}) and a low-density form (I_{al}). Thin ice samples, prepared by vapor deposition, were warmed up, revealing the following: (i) I_{ah} ice exists until 38 K; (ii) between 38 and 80 K, I_{ah} ice is gradually transformed into I_{al} ice, (iii) remaining in this form until 100 K. (iv) Above 100 K, I_{al} ice begins to transform into cubic crystalline ice and into a third amorphous form.[3] Kouchi and Yamamoto[4] reviewed amorphous ices under space conditions and found the following, depending on substrate temperature and deposition rate: (i) at $T < 140$ K, various forms of amorphous ice may be formed; (ii) at 140 K $< T <$ 165 K, the ice has a cubic structure; and (iii) at $T > 160$ K, a transition occurs toward a hexagonal structure. Data obtained with keV projectiles by Baragiola et al.[5] and with MeV ones by Brown et al.[6,7] show that sputtering yields are independent of ice temperature up to 60 and 100 K, respectively, but increase at higher temperatures. A similar temperature dependence of sputtering yields has been reported for photon- and electron-induced desorption.[8]

Conlan et al. observed the emission of three series of cluster ions, $(H_2O)_nH^+$, $(H_2O)_n^+$, and $(H_2O)_nOH^+$, from water ice at 100 K bombarded by high flux of 15 keV heavy projectiles (collisions in the nuclear regime).[9] The obtained mass spectra show particularly high yields for the $n = 4$ and 21 members, whose stability is attributed to a closed shell and to a clathrate-like dodecahedron structure,[10] respectively. They also compare their results with some others in the literature, discussing the relevant mechanisms.

Received: November 22, 2010
Revised: May 8, 2011

   dx.doi.org/10.1021/jp111152y | *J. Phys. Chem. C* XXXX, XXX, 000–000

The mass spectra of positive secondary ions ejected from water ice bombarded by a low flux of MeV projectiles (collisions in the electronic regime) are dominated by the series of cluster ions $(H_2O)_nH^+$.[11−13] The series $(H_2O)_n^+$ and $(H_2O)_nOH^+$ are practically nonexistent; furthermore, magic numbers are not or barely observed. These clusters can be understood as reaction products of the hydronium H_3O^+ and the aggregates $(H_2O)_n$; therefore, we prefer to use the notation $(H_2O)_nH_3O^+$ for their description.

Because water amorphous ices are commonly found on interstellar grains and continuously bombarded by cosmic rays, the production rate of H_3O^+ and $(H_2O)_nH_3O^+$ generated by light or by heavy ion impacts on such icy grains is important for chemistry in interstellar clouds. Recent experiments[12,14] on secondary ion emission from water ice, performed between 78 and 200 K, revealed strong variations of the secondary ion yield as a function of temperature, which were supposed to originate from phase transitions. However, subsequent measurements by Collado et al.[15] did not reproduce these yield variations.

The aim of the present work is to investigate how the structural changes of water ice influence the emission of secondary ions. The temperature dependence of secondary ion emission from water ice between 10 and 80 K had not yet been investigated; the present experiments are the first trial.

2. EXPERIMENTAL METHOD

The H_2O ice samples were irradiated by a 1.5 MeV N^{2+} beam of the Van de Graaff accelerator of the Pontifical Catholic University of Rio de Janeiro (PUC-Rio). Mass spectra of secondary ions emitted from the ice surface were measured by time-of-flight secondary ion mass spectrometry (TOF SIMS). The corresponding method employed in the current work has been described elsewhere[13] and is summarized below. The projectile ions penetrate the ice layer deposited on the target carrier, a thin Cu foil (200 $\mu g/cm^2$), from where the secondary ions are backward ejected with respect to the incident beam (backward sputtering process) and accelerated toward the stop detector. Secondary electrons produced at the target backside are accelerated to 2 keV and used to trigger start signals in a start detector. Both the start and the stop signals are feed into a start−stop time-to-digital converter (TDC) to generate TOF mass spectra of the secondary ions. After passing the target, the projectile ions travel a certain distance and impact a third detector, which is used to monitor the beam intensity and to measure by TOF the energy of each detected beam ion. The energy difference from the original beam energy, that is, the energy loss in the target, is used to determine the ice layer thickness d_{ice} by means of energy-loss calculation.[16] One essential improvement was added to the apparatus described in ref 13: the target holder, a Cu plate carrying the target foil, was connected to the head of a He cryostat. Both head and target are surrounded by a thermoshield at a temperature of about 45 K. The target is electrically isolated from the head and set to a voltage of +5 kV for providing the acceleration potential for positive secondary ions. Its temperature was calibrated as a function of the head temperature, which was measured by means of a Si diode.

2.1. Preparation of the Ice Layers. The H_2O ice was deposited on the target foil by blowing a weak flow of water vapor through a capillary onto this foil. Two ice targets were prepared, the first one (target #1) at T = 50 K with a growth rate of 0.35 nm/s, the second one (target #2), at T = 15 K with a growth rate of 1.3 nm/s. Under these conditions, the ice layers have distinct amorphous structures;[1,3,4] that is, ice condensed at 50 K is supposed to be a low-density amorphous ice, whereas that condensed at 15 K is a high-density amorphous ice. The residual gas in the spectrometer chamber condensed continuously on the surface of the ice samples. As investigated in detail using the current experimental data,[17] the H_2O rate of condensation was 0.30 ML/min and the volume content of organic impurities, mainly from pump oil, was about 3%. The background of organic impurity ions in the TOF mass spectra saturated within 15 min, when the corresponding H_2O layer thickness was 5 ML thick, showing that the ice layers were slightly contaminated by impurities. Because the rate of residual gas condensation was very low, the structure of the top and underneath layers should be amorphous. The mixture of 3% in volume is roughly equivalent to one organic molecule per 100 H_2O; this small concentration is probably not enough to change substantially transition temperatures. In particular, Kouchi et al. investigated a 1:5 mixture of CO and H_2O and found that the phase transition temperatures of the H_2O ice are the same as those for pure ice.[4] The residual gas was condensed with a deposition rate of 0.005 nm/s, a condition in which the additional water layers form amorphous ice, namely, I_{ah} below 30 K and I_{lh} above 70 K.[2] As a consequence, the residual gas layer should have the same structure as the bulk, at least below 30 K and above 70 K. In between these temperatures, the mixture of I_{ah} and I_{lh} occurs and the ice structure could be different; but also here, a gradual transition from I_{ah} to I_{lh} is expected. Because the temperature of the shielding is around 45 K, the temperature of the surface might be a little warmer than that of the bulk below this value, and inversely, above 45 K, it should be colder. The fact that the phase transitions are observed at the same (measured) temperatures, as those reported in refs 2 and 3, indicates that the temperature of the desorption layer is the same as that measured in the target holder. The enrichment of the top layer with organic impurities above 130 K due to H_2O sublimation and its influence on the emission of H_2O-specific ions are under analysis.[17] It has also been verified that, below 30 K, a second source of ice contamination appeared, which is condensation of N_2 from residual gas.

2.2. Absolute Ion Yields. Details on the absolute value measurement are given elsewhere.[15] Briefly, the goal is that all ions ejected from the target reach the surface of the microchannel plate detector. Considering the grid transmission and the relative sensitive area of the detector surface, the total efficiency was estimated to be 43% for the present stop detector. The acceleration and bias voltages have to be high enough to provide saturation in the yield measurement.

To get absolute values for measurements not acquired in the same conditions, all ion yields were first normalized to the $(H_2O)_{n=1-18}H_3O^+$ cluster yield measured at 80 K with 1.5 MeV N ions. Absolute yield values, given in (ions/impact) or (H_2O molecules/impact), of this cluster ion series were determined from previously measured absolute yields obtained at 80 K with N beams of energies between 0.5 and 1.7 MeV.[14,15] An empirical relation is needed to describe the dependence of the integral (summed over n = 1−18) cluster yields, Y_{cl}, on the stopping power fitting. The best obtained function was

$$Y_{cl} = 0.0010 \exp\left(\frac{S_e}{15.6}\right) \quad (1)$$

dx.doi.org/10.1021/jp111152y |J. Phys. Chem. C XXXX, XXX, 000–000

where $S_e = dE/dx_e$ is the electronic energy loss (in eV/Å units) of N ions in water ice taken from SRIM energy loss calculations.[16]

A power law dependence of yield on the stopping power $(S_e)^p$, where $p \sim 4$, has been reported in the literature.[18] As discussed in section 4.1, the current data agree with this result at high stopping power values, but $p = 3$ seems to be better throughout a larger range.

3. RESULTS

For the two targets, a series of TOF mass spectra were measured simultaneously as a function of time and ice temperature. The thickness of each ice layer, d_{ice}, deposited on the Cu foil was also measured during dosing and reached the maximum value of about 800 nm. For target #2, this remained approximately constant from 215 min, when dosing was stopped, until 305 min, when d_{ice} dropped rapidly due to sublimation above 130 K. Finally, 380 min after dosing, at $T = 215$ K, the ice layer disappeared.

The target ice #1 consists of low-density amorphous ice (Figure 1), in contrast with target ice #2, which is formed by a mixture of low- and high-density amorphous ices. The thicknesses of both ice layers were constant and about 800 nm. The dominant pattern of all spectra is the hydronium ion H_3O^+, followed by the $(H_2O)_{n+1}H^+$ cluster ion series, denoted here by $(H_2O)_nH_3O^+$ with n up to 45. Figure 1 exhibits the low mass region of the target #1 spectrum measured at $T = 50$ K. The spectrum correspond to an almost pure water ice, once the measurement started 1 min after dosing, when the layer of contaminant residual gas had only a thickness equivalent of 0.3−1.5 ML H_2O. The spectrum corresponding to target #2 was measured 160 min after dosing, when the background of organic impurity ions reached saturation (the residual gas layer has a thickness of about 50 ML). Some organic background lines came up. The differences between the two spectra related to the structural differences between the two samples are relatively small, but distinct, as seen from Table 1, which presents absolute yields measured at various temperatures with targets #1 and #2. The spectra acquired at temperatures below 30 K exhibit the cluster series $(H_2O)_nH_3O$ with intensities 1 order of magnitude higher than above 75 K. Small peaks that disappear above 30 K are attributed to condensed nitrogen. Table 1 shows the absolute yields measured at various temperatures in which the thickness of both ice layers were constant and about 800 nm.

For target #2, the ice sample was studied over a temperature range from 10 to 215 K within 6.3 h after dosing. The target temperature was increased step-by-step in units of 2 or 10 K. In total, 41 TOF spectra were measured, each one acquired during 300 s. Taking into account beam intensity variations, the spectra were normalized to the beam monitor rate or to the rate of start events. During these experiments, the rate of impacting N ions was about 650/s. Data displayed in Table 1 and Figure 1 show the absence of the OH^+ ion peak and the very small yield of H_2O^+ species compared to the H_3O^+ one. Actually, the yields of the $(H_2O)_nOH^+$ and $(H_2O)_n^+$ series are negligible with respect to the $(H_2O)_nH_3O^+$ one. As explained in the Figure 1 caption, the satellite peak is an electronic artifact. The main peaks are attributed to the $H_2(H_2O)_nH^+$ series, formed by the attachment of molecular hydrogen (adsorbed in the ice surface) to $(H_2O)_nH^+$ or $(H_2O)_nH_3O^+$ secondary cluster ions. The other small peaks are due to organic contaminants.

Figure 2a,b shows, as a function of time/temperature, the yields of the $(H_2O)_nH_3O^+$ cluster ions and the observed H_2O-specific

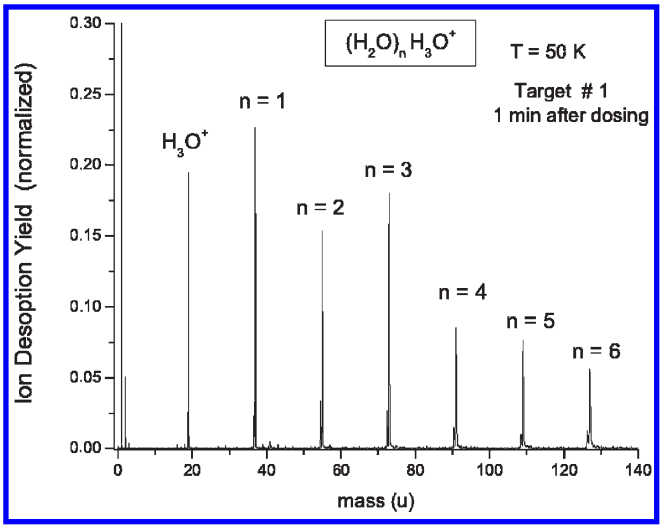

Figure 1. TOF mass spectrum: target #1 taken 1 min after dosing. All mass lines show, on the left side, a small satellite peak caused by electronic reflections of the start pulses: the time interval to the main peak is constant; up to 100 u clusters, the mass lines $n - 1$ are separated from this satellite peak.

Table 1. Absolute Ion Yields (Ions/Impact) for the Two Targets Measured at Various Ice Temperatures with 1.5 MeV N^{2+} Ions. Both ice layers were bombarded by 1.5 MeV N^{2+} ions and their thickness were about 800 nm during the measurements.

secondary ion	target #1 Y (50 K)	target #2 Y (50 K)	target #2 Y (10−30 K)	target #2 Y (80 K)
H^+	0.047	0.070	0.063	0.049
H_2^+	0.005	0.008	0.004	0.010
H_2O^+	0.0004	0.002	0.027	0.0012
H_3O^+	0.018	0.031	0.25	0.012
$(H_2O)H_3O^+$	0.030	0.054	0.26	0.021
$\Sigma(H_2O)_{n=1-29}H_3O^+$	0.236	0.335	1.49	0.214
$C_4H_9^+$	0.0004	0.005	0.013	0.002
$\Sigma C_nH_m^+$	0.026	0.147	0.69	0.088

ions, respectively. The evolution of the ice thickness, d_{ice}, is also presented; note that it decreases above 157 K, clearly after the start of decreasing of the cluster ion yields at ∼140 K.[17] To provide a better data visualization, the ion desorption yields of clusters with sizes from $n = 2$ to 19 are grouped into $n = 2-4$, $n = 5-8$, $n = 9-13$, and $n = 14-19$ and displayed as four curves: n = ⟨3⟩, ⟨6⟩, ⟨11⟩, and ⟨16⟩.

Above 140 K, the yields of all cluster ions drop rapidly and vanish after 300 min, around 160 K. In the data presented in Figure 2a,b, one can distinguish four types of secondary ions:

1. H^+ and H_2^+ ions. Their main characteristics are the following: (i) As the temperature rises, the yield evolution for the two species does not exhibit large variations. (ii) Over the whole temperature range from 10 to 216 K, the H^+ yield declines steadily by a factor 2.5. (iii) Both species are commonly observed in secondary ion mass spectra and show up even with ion etched metal surfaces at vacuum pressures below 10^{-10} mbar,[19] which is a situation where they originate from residual gas adsorption.

dx.doi.org/10.1021/jp111152y |J. Phys. Chem. C XXXX, XXX, 000–000

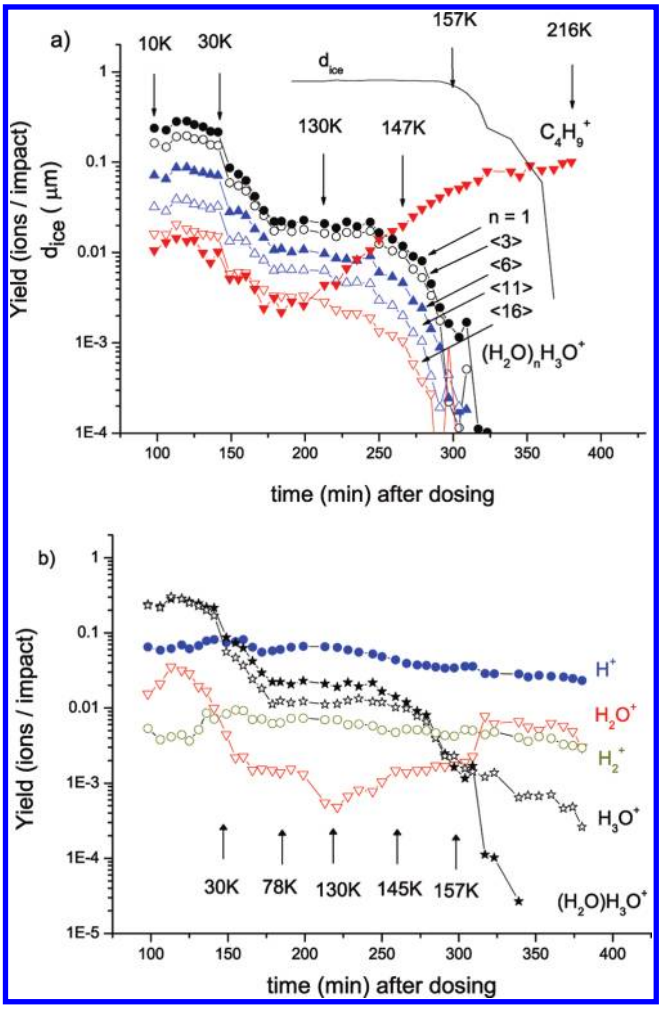

Figure 2. Yields of secondary ions ejected from water ice by a 1.5 MeV N^{2+} beam as a function of the warming up time. (a) Ion yield evolution of cluster ions $(H_2O)_nH_3O^+$ and of the organic impurity ion $C_4H_9^+$. The data points of the curves designed with $n = \langle 3\rangle$, $\langle 6\rangle$, $\langle 11\rangle$, and $\langle 16\rangle$ are averaged yields (see text). The ice layer thickness d_{ice}, measured with the help of the beam-energy loss, is also presented (solid line). (b) Yield time dependence of the H_2O-specific ions, H^+, H_2^+, H_2O^+, and H_3O^+, and, for comparison, of the first cluster ion $(H_2O)H_3O^+$.

2. The H_2O-specific ions: H_2O^+, H_3O^+, and $(H_2O)_nH_3O^+$. The main characteristics of their yields are the following: (i) They all present a flat maximum between 10 and 30 K. (ii) Afterward, they decrease gradually in the 30−80 K interval by 1 order of magnitude. (iii) They remain almost constant within the 80−125 K interval. Subsequently, the yields of cluster species start to decrease slowly, while H_3O^+ stays constant until 140 K, the H_2O^+ yield starts to increase. (iv) They drop finally at 157 K to zero or, in the case of H_3O^+, to very low values. The H_2O^+ yield keeps increasing slowly up to 160 K, where it rises suddenly by a factor 4. The increase coincides with the complete disappearance of the cluster ions. This disappearance occurs when the ice layer is still several hundred nanometers thick. At about 130 K, sublimation of H_2O ice surpasses condensation rest gas and the top surface layer becomes more and more enriched with organic impurities when time and temperature elapse. For instance, as seen in Figure 2a, the yield of the organic ion $C_4H_9^+$ exhibits a strong increase above 130 K, whereas the yield of the $(H_2O)_nH_3O^+$ cluster ions decreases in accordance to (H_2O) depletion of the top surface layer. The phenomena will be discussed in ref 17. (v) The $(H_2O)_n^+$ ion yields are found to be negligible (at the noise level).
3. The organic impurity ions $C_nH_m^+$. They are formed from the condensed residual gas.
4. The ions N^+, N_2^+, NH^+, NO^+, and $(H_2O)_mNO^+$ with m = 1, 2, and 3. They stem from nitrogen being mixed in small quantities to the residual gas.

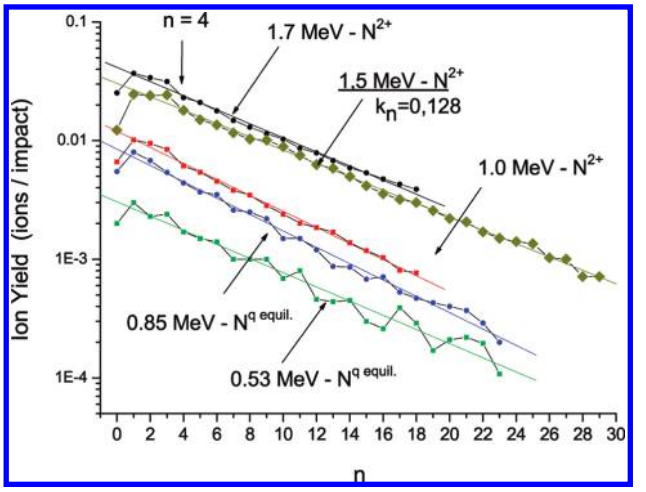

Figure 3. Cluster distribution of $(H_2O)_nH_3O^+$ ions, measured with 1.5 MeV N^{2+} projectiles at T = 80 K in the present work, is compared with four distributions obtained recently under similar conditions at beam energies of 0.53, 0.85, 1.0, and 1.7 MeV.[14,15] The charge state of the nitrogen ions was $q = 2+$ (backward sputtering) or $q = q_{\text{equilibrium}}$ (transmission sputtering). The curve measured with a 1.5 MeV N^{2+} beam was interpolated using the dependence of ion yields on the electronic energy loss given by eq 1.

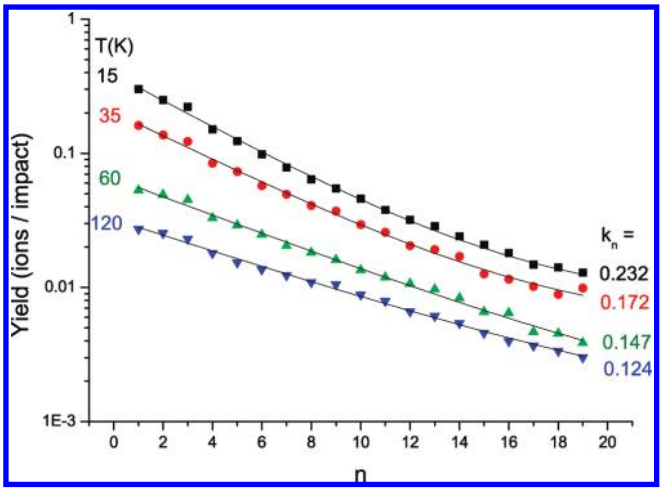

Figure 4. $(H_2O)_nH_3O^+$ cluster ion yield distributions measured at temperature ranges of T = 10−20, 30−40, 50−70, and 80−130 K. In Figure 3, average data are displayed through four lines approximately exponential. The obtained points are fitted to exponential functions $Y_0 \exp(-k_n n)$, from which the slope parameters k_n are derived.

Figures 3 and 4 present the cluster ion yield distributions as a function of size, for different projectile energies and ice temperatures, respectively. All the cluster distributions were fitted by a

dx.doi.org/10.1021/jp111152y |J. Phys. Chem. C XXXX, XXX, 000–000

decreasing exponential function:

$$Y = Y_0 \exp(-k_n n) \quad (2)$$

The choice of this function is essentially based on the good agreement in the distribution of the cluster size in condensed gas systems.[20−22] Other functions[19](the sum of two exponentials, power law and log-normal) have been used for fitting cluster mass distributions of other target material or for higher stopping power projectile−target systems. For the current and similar[15] data, the single exponential shows a very good agreement and presents the advantage of the lowest number of free parameters.

Analysis of Figure 3 data shows that all distributions are essentially parallel to each other, which means that the slope parameter k_n is the same for all impact energies, their mean value being 1.44 ± 0.02. The first point of the distribution (n = 0) corresponds to the yield of the hydronium H_3O^+. Systematically, it does not fit to the distribution, which is a clear indication that the links (hydrogen bridges, in this case) among water molecules should define the behavior of the yield distribution. Another trend extracted from this data is the dependence of ion yield on the projectile energy: all cluster yields increase as the nitrogen ion energy increases.

The dependence of the cluster ion yield on the ice temperature can be examined via Figure 4, which shows a comparison of four cluster distributions measured in the T = 10−130 K interval. The important and unexpected result is that the desorption ion yield decreases when the water ice is warmed up. Moreover and contrary to the dependence on projectile energy variations (when the distribution slope is constant), the slope parameters k_n decrease from 0.232 to 0.147 with rising temperature; that is, the number of small clusters ejected per impact decreases faster than that of large ones. The data presented in Figure 4 are not fitted by a single exponential. This "artifact" occurs because of the k_n determination. All the spectra acquired during the warming up process were divided into four groups and averaged for reducing statistical fluctuations. Because the sum of exponentials is not an exponential, the fitting was performed by adding two exponentials with very different amplitudes. The presented k_n values correspond to the dominant one.

4. DISCUSSION

4.1. Sputtering of $(H_2O)_nH_3O^+$ Cluster Ions by MeV N Ions. Concerning cluster emission mechanisms, it has been suggested that the ejected $(H_2O)_nH_3O^+$ are ionized preformed $(H_2O)_n$ clusters. That means that, in the surface layer of water ice, preformed clusters $(H_2O)_n$ exist, which can become ions during the desorption process by the production of H^+ or H_3O^+ inside the cluster or by H^+ or H_3O^+ capture.[15] The following analysis of the present experimental data changes this picture to a certain extent.

In Figure 5, the yields of cluster ions $(H_2O)_nH_3O^+$ measured for five energies of nitrogen ions are displayed as a function of the electronic energy loss $S_e \equiv (dE/dx)_e$ and compared with the total (neutral + ionic) sputtering yields. Figure 3 presents the corresponding cluster ion yield distributions. The total sputtering yields were taken from a compilation of sputtering yields of water ice bombarded by oxygen-like projectiles presented by Shi et al.[8] The number of H_2O molecules assembled in the cluster ions accounts for about 97% of the total ion yield, and therefore,

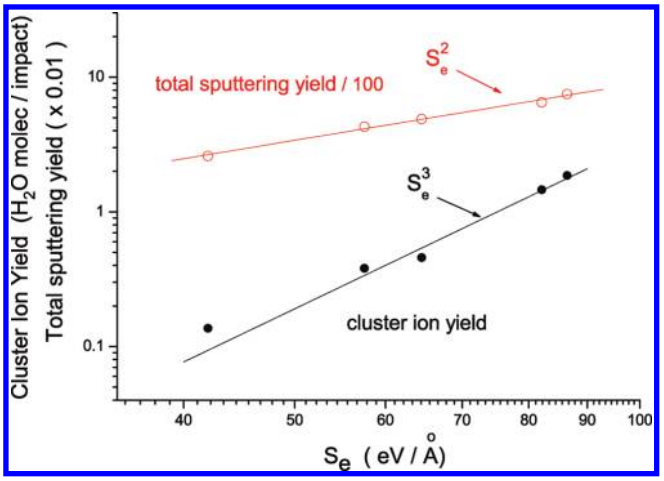

Figure 5. Comparison between total sputtering[8] and ion yields of water clusters corresponding to bombardment of MeV N ions on water ice at a temperature of 80 K.

the cluster ion yield represents approximately the total yield of desorbed ionic species. The solid lines, being adjusted to the data points, reveal a second and third power dependence of the yields on S_e.

4.1.1. Sputtering of Water Ice by MeV Ions. Beyond the Bohr velocity, which is equivalent to an energy of 25 keV/u, a heavy ion deposits most of its energy in electronic excitation of the target solid. The value of S_e is typically more than 2 orders of magnitude larger than S_n, the nuclear energy loss. About two-thirds of the deposited energy goes into the kinetic energy of secondary electrons, which generate ternary electrons and excitation. Finally, all the so-called δ electrons cool down by vibrational or rotational excitation of molecules and by elastic momentum transfer collisions with atoms. In insulators, such as H_2O ice, the electronic excitations can lead to repulsive states, which cause, at the target surface, particle ejection. The number of electronic excitations is proportional to S_e; that is, at low S_e, the sputtering yield is, in fact, linear in S_e. When the density of excitations is high, cooperation between close excitation events along the nuclear track enhances the sputtering yields; the yields scale with the second or a higher power of S_e.[20] In the case of water ice, a scaling of yields like $(S_e)^2$ has been reported for oxygen-like ions having energies of 1−200 keV/u.[8]

At high excitation density, a cylindrical zone around the track becomes continuously energized. In the radial direction, the energy per molecule deposited primarily by δ electrons decreases with $1/r^2$, which has been proved for water ice experimentally as well as by model calculations.[23] Therefore, most of the primarily deposited energy is concentrated close to the track. The evolution of this highly energized central zone in the radial direction and up to the surface (where the sputtering takes place) has been the subject of several theoretical studies,[24] which are usually classified as thermal models or expansion models. In the present case, for water ice and relatively low energy loss, thermal sputtering seems to be the appropriate model. Calculation[25] shows that, in the case of 1.5 MeV N ions, about 98% of S_e (equal to 260 eV/ML) amounts are primarily within a radius of 1 nm and the mean energy density within this radius is about 8 eV/molecule. This energy dissipates rapidly (eventually by nonlinear energy transfer) into the material surrounding the track. A larger zone is heated and locally thermalized. From the corresponding thermal sputtering models,[24] it appears that

dx.doi.org/10.1021/jp111152y |J. Phys. Chem. C XXXX, XXX, 000–000

thermal sputtering also scales with $(S_e)^2$. In the case of water ice, the energized material around the track can become liquid or gaseous and expands at the surface into vacuum as a plume of water molecules.

Mass-resolved sputtering experiments were performed by Brown et al.,[7] who irradiated D_2O ice with 1.5 MeV He^+ ions. They observed a constant D_2O yield between 10 and 140 K, and a rising yield, when sublimation began. Clustered D_2O molecules, even $(D_2O)_2$, were not reported. So far, there is no evidence that the flux of sputtered H_2O molecules contains any neutral clustered $(H_2O)_n$. Neutral water clusters have been observed, for example, in molecular beam experiments from supersonic expansion in vacuum[26] or IR laser irradiation of water ice,[27] but it is shown that there is an increase of the decaying pathways of excited clusters as the cluster size increases. Therefore, we expect that, due to the high density, the energized material surrounding the nuclear track contains certainly clustered H_2O molecules, which redistribute their hydrogen bonds rapidly depending on its temperature. When the excited material expands into vacuum like a plume, excited neutral clusters left in the plume probably decay.

The sputtering yield measured with 1.5 MeV He^+ ions as a function of ice temperature is constant between 10 and 120 K and increases toward higher temperatures, as sublimation starts to set in.[7,17] Cooper and Tombrello[18] also reported a temperature-independent H_2O yield between 10 and 60 K by employing 1.6−25 MeV ^{19}F beams on H_2O films.

4.1.2. Emission of Cluster Ions $(H_2O)_nH_3O^+$. As seen in Figure 5, the ionic fraction of the sputtering yield is about 3 orders of magnitude smaller than the total sputtering yield. The later scales with the second power of S_e, the ionic fraction with the third power of S_e. Because the number of ionizations per length unit of the nuclear track is proportional to S_e, also the probability to ionize a cluster $(H_2O)_n$ is proportional to S_e.[20] This leads to a power dependence of the cluster ion yield one unit higher than the power of the total sputtering yield.

For S_e values to be 1 order of magnitude higher than those of MeV N ions, Hedin and co-workers[28] observed that the power of the S_e dependence of molecular ion yields increased with molecular size, that is, the larger the molecular ion, the higher the power of the S_e dependence. Such an effect is not found for the five cluster distributions presented in Figure 3, where the yield curves are remarkably parallel and the slope parameter k_n is constant and not depending on S_e. When preformed clusters are traversed by the primary ion, they are destroyed via strong Coulomb interaction. Therefore, concerning detected cluster ions, they may be preformed only if their ionization by electron impact occurs beyond the nuclear track. Their yield should depend on cluster size: the larger the cluster volume, the higher the ionization probability. This should cause a cluster size effect on the cluster mass distributions, particularly, when the size of large clusters becomes comparable to the range of the δ electrons. For the measured five cluster distributions, a size effect has not been observed; therefore, we suggest that the cluster ions found in the mass spectra do not correspond to $(H_2O)_n$ clusters of the same size present before ionization and desorption. According to the high density of the material around the nuclear track, ionization by δ-electron impact occurs on water molecules being bound to neighboring water molecules by hydrogen bridges, that is, on clustered water molecules. These cluster ions may not have the final size observed in the mass spectra, because, as long as the number of collisions is high, they change their size via redistribution of hydrogen bonds. The final size is reached after the plume of sputtered material is expanded into vacuum. The fact that only cluster ions (i.e., not neutrals) are observed in the flux of sputtered material suggests that the H_3O^+ ion stabilizes the cluster. The ionization process can be described by

$$e + (H_2O)_n \rightarrow 2e + (H_2O)_n^{*+} \quad (3)$$

The $(H_2O)_n^{*+}$ cluster ion dissociates in ice as

$$(H_2O)_n^{*+} \rightarrow (H_2O)_{n-2}H_3O^{*+} + OH^{\bullet} \quad (4)$$

or as

$$(H_2O)_n^{*+} \rightarrow (H_2O)_{n-1}H^+ + OH^{\bullet} \quad (5)$$

where $OH^{\bullet}$ represents a free radical. Another way to produce H_3O^+ is

$$H^+ + H_2O \rightarrow H_3O^+ \quad (6)$$

The situation of cluster ion production in water ice by δ-electron impact of clustered H_2O molecules is similar to electron-beam-induced ionization of molecular beams.[29] In this case, a beam of water vapor is irradiated by electrons having energies of some tens of electronvolts, an energy range similar to that of δ electrons; the molecular beam consists of neutral (H_2O_n) clusters, which, contrary to the clusters in the excited track material, are relatively cold and do not decay during flight.

The ion mass spectra reported by ref 29 are quite similar to those obtained with MeV N ion bombardment of water ice. A series of protonated $(H_2O)_n$ are almost exclusively formed. The variation of cluster ion yields with cluster size depends on the conditions used to form the molecular beam. The cluster size is determined by the efficiency with which clusters can increase in size and remain stable. At high pressures, as in the present case of a hot, very dense plume of water molecules, the number of collisions will be high, favoring the increasing of the water cluster size and collisional cooling. At low pressures, the tendency to form large clusters is smaller, and the slope parameter k_n is larger than at high pressures. In the excited material around the nuclear track, the pressure is extremely high; thus, the slope parameter $k_n = 0.14 \pm 0.02$, determined as a mean value for the cluster distributions observed in the present work, (see Figure 3) can be considered as a lower limit reached with very high molecular beam pressures.

The hydronium H_3O^+ is located in the highly energized zone of the nuclear track, where the desorption process develops. In water ice, this process is probably not very different from sputtering of frozen or liquid water by keV heavy ions. In both cases, the observed secondary ion mass spectra are quite similar to those of the present work. The observed pattern for the frozen water target[21,30] is $(H_2O)_nH_3O^+$, and for the liquid water target,[31] it is $(H_2O)_nOH^-$ (the spectrum of positive ions was not investigated). The latter series of negative clusters was also found by Collado et al.,[15] with MeV N ions. At keV incident energies, sputtering is supposed to be initiated by atomic collision cascades. The complex movement of an ion like H_3O^+ in the collision cascade region and its attachment to water molecules have been investigated using molecular dynamics calculations.[30] Experiments[9] as well as the molecular dynamics calculations prove the ejection of water solvated H_3O^+. In fact,

dx.doi.org/10.1021/jp111152y |J. Phys. Chem. C XXXX, XXX, 000–000

mass spectra obtained with a high flux of 15 keV heavy cluster ion projectiles[9] show emission of $(H_2O)_n^+$ secondary species with yields larger than the $(H_2O)_nH_3O^+$ species; after a fluence of 3×10^{13} ions/cm^2, the yields of the more fragile $(H_2O)_n^+$ clusters became lower than the $(H_2O)_nH_3O^+$ ones. The $(H_2O)_n^{+*}$ ions are claimed to be unstable, but the presence of the solid surface provides a means for their de-excitation.

Some model calculations for proton hydration[32] predict enhanced stability near $n = 21$, where a charged hydronium unit is located in the interior of a $(H_2O)_nH^+$ for $n = 20$, 21, and 22. Small yield increases at $n = 20$ and 21 were observed in mass spectra of cluster ions $(H_2O)_nH^+$ measured by Matsuo et al.,[33] who irradiated water ice at $T = 15$ K with 1.5 MeV Ar^{13+} ions. The present cluster distributions for $n > 4$ are almost identical with those measured by Matsuo et al., but enhanced yields at any $n > 4$ were not found (see Figure 3). Only the yield of $(H_2O)_3H_3O^+$ is slightly enhanced.

The peaks of the cluster ion masses shown, for instance, in Figure 1 are not broadened and do not show shoulders. That means that delayed ion emission or metastable decay during flight does not occur. The cluster ions ejected from the water ice are "cold"; internal energy has been eventually conducted away by frequent collisions. Evaporation of H_2O molecules leads to particularly stable clusters, which were not observed.

From ref 8, a total sputtering yield of 650 H_2O molecules/impact for 1.5 MeV N ions on water ice can be estimated. The corresponding cluster ion yield given in Table 1 (ion yields multiplied by the mean number of H_2O molecules of the cluster distribution) is 0.33% of the total sputtering yield. A 1.5 MeV N ion traversing water ice at 80 K generates on average 13 positive ionizations/ML by electron impact.[20] The secondary electrons have a kinetic energy of some tens of electronvolts, to be compared to 11 eV, the energy needed to ionize a water molecule in ice. Assuming that the five top monolayers of the ice target contribute to sputtering, the primary ionizations are 10% of the total sputtering yield. That means that the most produced ions have a very small survival probability, only 3%. Neutralization by δ-electron capture is hardly possible. The δ electrons lose their kinetic energy by scattering and become bound to atoms or molecules, from were they can recombine with holes, that is, positive species.

The production of H^+ and OH^- requires 16 eV, but recombination of such ion pairs is quite probably due to the close proximity of these ions. Recently, negative ion spectra were measured with 0.83 MeV N ions on water ice.[15] The yield of the negative ions based on OH^- was found to be 45 times smaller than the corresponding positive ion yield.

4.2. Temperature−Time Dependence between 10 and 125 K. To compare the temperature dependence of all desorbed ion species, the yields of the $(H_2O)_nH_3O^+$ cluster ions, nitrogen-containing contaminants $N_nO_mH_l^+$, and organic impurity ions $C_nH_m^+$ were summed. These integral yields as a function of the ice temperature are presented in Figure 6. The yields are integrated from $n = 1-19$ for water clusters and for all observed ions of organic impurities having a mass between 27 and 500 u. In target #2 (Figure 6 and Table 1), the integral yield of the cluster ions varies moderately in the temperature range of 10−30 K, decreases between 30 and 75 K by factors up to 20, and remains constant until 130 K. Over the whole temperature range, the basic structure of the ice produced by vapor deposition (see section 2) should be amorphous. The transition regime of 30−75 K coincides with a temperature range, where a phase transition between two forms of amorphous water has been observed.[2]

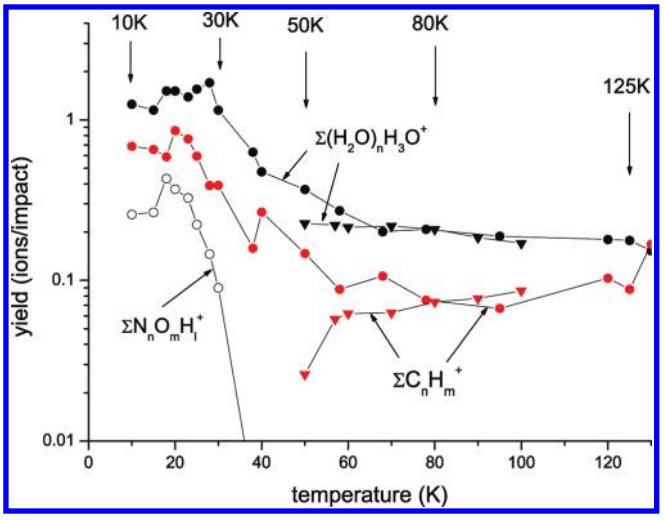

Figure 6. Integral yields of cluster ions $(H_2O)_nH_3O^+$, organic impurity ions $C_nH_m^+$, and nitrogen-containing impurity ions $N_nO_mH_l^+$ measured with target #1 (triangles) and target #2 (dots) as a function of ice temperature. The yields of the cluster ions were summed from $n = 1-19$. The measurements for both targets #1 and #2 started 1 and 100 min after dosing.

According to Jenniskens et al.,[2,3] the water vapor deposited below 34 K forms the high-density amorphous ice (I_{ah}), which changes gradually into low-density amorphous ice (I_{al}) when the ice is warmed up from 38 to 65 K. The I_{ah} ice density is about 15% higher than that of I_{al}. Such an increase of density leads to a higher specific energy loss but cannot result in a substantially higher sputtering yield. Brown et al.[6,7] proved that the total sputtering yield of water ice remains constant at temperatures from 10 to 120 K. Assuming that the change of ion yields is related to ionization, the production and recombination of electron−hole pairs should occur in solid ice. In the two amorphous forms of ice, apart from a small density effect, the production rate of electron−hole pairs should be the same. In the case of I_{al}, the fraction of not neutralized ions accounts for about 0.7% of the ionizations, and in the case of I_{ah}, it accounts for 4.5%. This difference of ion yields corresponds to a quite small change of neutralization, probability by 4%. Therefore, a small change in electron conductivity or mobility may have a large influence on the number of ions, which are not neutralized. The decrease of ion yields between 30 and 75 K is also observed for the integral yield of ions due to organic impurity ions: Thus, the reduction of ionization going from I_{ah} to I_{al} concerns not only H_3O^+ but also the organic ions.

Jenniskens and Blake[2,3] studied amorphous water ice by electron diffraction and confirmed that the ice below 30 K restructures rapidly. On the basis of this unexpected molecular rearrangement, they proposed that the water ice has a high mobility at these temperatures, fast redistribution of hydrogen bonds being faster in I_{ah} ice than in I_{hl} ice.[34] Because the hydrogen bonds in I_{ah} redistribute rapidly and continuously, the mobility of electrons and holes decreases, and the neutralization rate by electron−hole recombination is reduced, increasing both the H_3O^+ density along the nuclear track and the $(H_2O)_nH_3O^+$ desorption yield.

In Figure 6, the integral ion yields obtained originally with I_{ah} ice (target #2, dots) are compared with those measured with I_{al} ice (target #1, triangles). The measurements with target #1 started with low-density amorphous ice at 50 K and show that

dx.doi.org/10.1021/jp111152y |J. Phys. Chem. C XXXX, XXX, 000–000

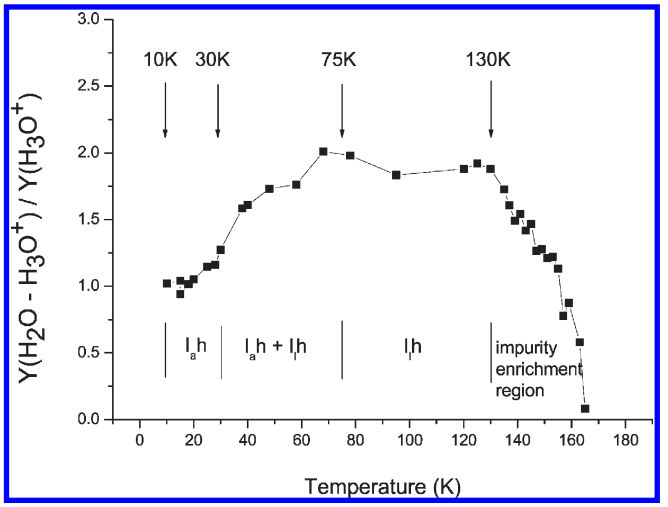

Figure 7. Ratio of $Y((H_2O)H_3O^+)/Y(H_3O^+)$ plotted versus ice temperature. The effect of impurity enrichment in the top layer of the ice sample will be discussed in ref 17.

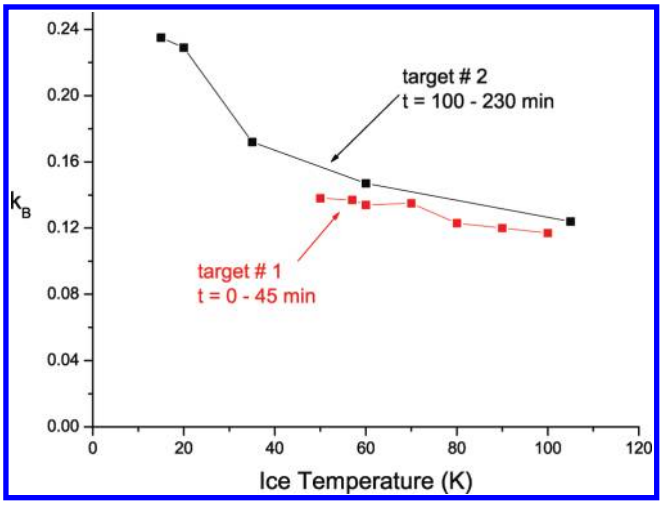

Figure 8. Slope parameter k_n measured at different temperatures with two ice targets, #1 condensed at 50 K and #2 condensed at 15 K.

a substantial decrease of the integral cluster ion yields toward higher temperatures is not observed: at 50 K, both yields differ by a factor of 1.4 (see Table 1). This is proof that, at this temperature, the ice of target #2 still consists partially of I_{ah} ice. Note that the integral yield $C_nH_m^+$ of target #1 exhibits a steep increase at the beginning of the measurement. This is attributed to the rapid modification from a very low impurity concentration in the top layer, 1 min after stopping the dosing, to an impurity enrichment saturation, after 15 min.

The hydronium ion H_3O^+ exhibits a peculiar behavior, which is illustrated in Figures 2b and 7. In the temperature regime between 75 and 130 K, when the ice has the I_{al} form, the H_3O^+ yield is a factor 1.9 smaller than that of the first cluster $(H_2O)H_3O^+$, whereas between 10 and 30 K, where I_{ah} ice is present, the yields of both ions are almost equal (ratio of 1.05). The transition regime occurs within the 30−70 K interval. This demonstrates that, during the cluster formation process in I_{ah} ice, a relatively smaller fraction of H_3O^+ ions becomes water solvated than in I_{al} ice, a possible consequence of the substantially higher production rate of H_3O^+ in I_{al} ice.

Figure 4 shows a comparison of four $H_2O_nH_3O^+$ cluster distributions, measured at T = 15−120 K, that is, the same temperature regime in which ion emission occurs from high- as well as low-density amorphous ice. The exponentially decaying distributions are characterized by slope parameters k_n, whose values are displayed in Figure 8 as a function of the ice temperature. Data obtained with the two ice targets are presented. The parameter k_n generally decreases with rising temperature, but there is a distinct difference concerning high- and low-density amorphous ice at T = 15−35 K and T = 60−120 K, respectively: k_n measured for I_{ah} is a factor of 1.7 larger than k_n measured for I_{al}. The size of the clusters emitted from I_{ah} ice is slightly shifted to smaller values compared with the size of those from I_{al} ice; that is, the mean number of molecules/cluster changes from 8.0 to 9.5. This effect could be related again to the higher mobility of molecules in I_{ah} ice.

4.3. H^+ and H^{2+}. The hydrogen ions observed in mass spectra of the current experiment are produced in the uppermost molecular layers and stem mainly from adsorbed residual gas, that is, from water and organic impurities. An argument to support this statement is that H^+ and H^{2+} ions are emitted from the metallic substrate prior to the ice deposition with comparable intensities. The H^+ is produced by direct Coulomb interaction of the N^{2+} beam ions with hydrogen-containing molecules. The H^+ can react with atomic or molecular hydrogen in the infratrack, the highly energized zone very close to the primary ions path, to form H^{2+}. Both hydrogen ions are directly ejected out of the more or less gaseous central part of the nuclear track. This has been proved by investigations of the energy and angular distributions of both ions.[35] Because they experience the transient positive charging of the infratrack, their kinetic energy is substantially higher than that of most other ions, also of the cluster ions. In Figure 2a, the H^+ emission is not sensitive to the various structural forms of the water ice; even enrichment with organic impurities above 130 K has no substantial influence. An exception is its yield reduction between 10 and 30 K, which may be interpreted that a certain fraction of H^+ ions is consumed by reactions with nitrogen, a residual gas component that sublimates above 30 K.

5. SUMMARY AND CONCLUSIONS

The present study of ion emission from water ice by heavy ion irradiation is devoted to structural changes of the ice occurring with time when its temperature rises. The measurements of ion yields started at an ice temperature of 10 K and continued for 4.7 h, increasing the temperature, step-by-step, up to 216 K, when the water ice had disappeared from the target by sublimation. The mass spectra of the secondary ions consist of H_2O-specific ions, particularly, hydronium H_3O^+, and cluster ions $(H_2O)_nH_3O^+$, and of impurity ions, mainly from organic molecules. The $(H_2O)_n^+$ series[9] observed for nuclear sputtering is barely seen, and members of the $H_2(H_2O)_nH^+$ satellite series have relatively small yields.

First, the yields of clusters $(H_2O)_nH_3O^+$ are compared with total sputtering yields taken from the literature.[8] The total sputtering yield scales with the second power of S_e, whereas the yield of the ionic clusters, a very small fraction (0.3%) of the total sputtering yield, is proportional to S_e^3. This third power can be understood by the fact that the number of ionizations is linear in S_e. Because the shape of the cluster distributions measured with 0.53−1.7 MeV N ions does not change with S_e, we

dx.doi.org/10.1021/jp111152y |J. Phys. Chem. C XXXX, XXX, 000–000

concluded that the ejected cluster ions are not produced by ionization of preformed $(H_2O)_n$ aggregates. They are formed inside the excited material around the nuclear track by δ-electron impact on H_2O molecules being bound to neighboring water molecules. The material probably becomes gaseous and expands into vacuum. The ionization process is comparable with cluster ion formation in molecular beams,[29] which are irradiated by electron beams. The cluster ions are formed by hydration of $(H_2O)_n$ or $(H_2O)_nH^+$ being produced by δ-electron impact of $(H_2O)_n$. Because clusters $(H_2O)_n$ have, so far, not been found in the flux of sputtered particles, which consists mainly of H_2O molecules, it should be considered that the desorbed $(H_2O)_n$ excited clusters rapidly evaporate. When the clusters are formed by hydration of H_3O^+, the hydronium ion stabilizes the momentary cluster configuration.

The mass spectrum analysis reveals that the $(H_2O)_nH_3O^+$ cluster ion yields are highest in the temperature range of 10−30 K, decrease gradually until 65 K by a factor of 6.5, and remain constant until about ∼125 K. This decrease is unexpected, in the sense that the higher the temperature, the higher the sublimation rate. The ion desorption mechanism may be distinct from the thermal sublimation. We propose that it should be connected to the phase transition from the high-density form of amorphous ice (I_{ah}) to the low-density one (I_{al}). The observed ion yields seem to follow three water ice amorphous phases: in the 10−30 K interval, they are related to a pure I_{ah}, in the 38−75 K interval, to a mixture of I_{ah} and I_{al}, and in the 80−130 K interval, to pure I_{al}. For ion emission, the essential feature of I_{ah} is that ionizations produced along the nuclear track have a higher survival probability than those produced in I_{al}. This can be explained by the peculiar structure of I_{al} resembling liquid water rather than crystalline ice. Compared with solid ice, fast redistribution of hydrogen bonds, typical for liquid I_{ah}, diminishes charge carrier transport and neutralization of ions, particularly of H_3O^+, which is the crucial reaction partner for the formation of $(H_2O)_nH_3O^+$. In addition, impurity ions experience the reduced neutralization probability: their temperature/time dependence of yields follows that of the cluster ions.

At T = 10−30 K, the yield of H_3O^+ is relatively higher compared with the cluster yields, probably due to the enhanced production rate of H_3O^+ in I_{ah} ice. The yield ratio of $Y((H_2O)H_3O^+)/Y(H_3O^+)$ measured as a function of time/temperature exhibits clearly the three amorphous regimes. Above 130 K, sublimation of the water ice causes rapid enrichment of the top layer of the surface with organic impurities, which will be the subject of a future article.[17] Because this ratio is easy to measure, it offers a reliable method to identify structural changes of water ice, such as phase transitions.

AUTHOR INFORMATION

Corresponding Author

*E-mail: abarros@if.ufrj.br.

ACKNOWLEDGMENT

The Brazilian agencies CNPq, CAPES, and FAPERJ provided partial support for this study.

REFERENCES

(1) Petrenko, V. F.; Whitworth, R.W. *Physics of Ice*; Oxford University Press: New York, 1999.

(2) Jenniskens, P.; Blake, D. F.; Wilson, M. A.; Pohorille, A. *Astrophys. J.* **1995**, *455*, 389.

(3) Jenniskens, P.; Blake, D. F. *Astrophys. J.* **1996**, *473*, 1104.

(4) Kouchi, A.; Yamamoto, T. *Prog. Cryst. Growth Charact.* **1995**, *30*, 83.

(5) Baragiola, R. A.; Vidal, R. A.; Svendsen, W.; Schou, J.; Shi, M.; Bahr, D. A.; Atteberry, C. L. *Nucl. Instrum. Methods Phys. Res., Sect. B* **2003**, *209*, 294.

(6) Brown, W. L.; Augustyniak, W. M.; Lanzerotti, L. J.; Johnson, R. E.; Evatt, R. *Phys. Rev. Lett.* **1980**, *45*, 1632.

(7) Brown, W. L.; Augustyniak, W. M.; Marcantonio, K. J.; Simmons, E. H.; Boring, J. W.; Johnson, R. E.; Reimann, C. T. *Nucl. Instrum. Methods Phys. Res., Sect. B* **1984**, *1*, 307.

(8) Shi, M.; Baragiola, R. A.; Grojean, D. E.; et al. *J. Geophys. Res.* **1995**, *100*, 387.

(9) Conlan, X. A.; Fletcher, J. S.; Lockyer, N. P.; Vickerman, J. C. *J. Phys. Chem. C* **2010**, *114*, 5468–5479.

(10) Wei, S.; Shi, Z.; Castleman, A. W., Jr. *J. Phys. Chem.* **1991**, *94*, 3268.

(11) Wien, K. In *Proceedings of the International Workshop on PDMS and Marine Organic Chemistry*; Hilf, E. R., Tuszynski, W., Eds.; World Scientific: London, 1989; p 82.

(12) Matthäus, R.; Moshammer, R. In *PDMS and Clusters*; Hilf, E. R., Kammer, F., Wien, K., Eds.; Lecture Notes in Physics; Springer-Verlag: Berlin, **1986**; Vol. *269*, p 241.

(13) Farenzena, L. S.; Collado, V. M.; Ponciano, C. R.; da Silveira, E. F.; Wien, K. *Int. J. Mass Spectrom.* **2005**, *243*, 85.

(14) da Silveira, E. F.; Wien, K. Van de Graaff Lab. of PUC-Rio, Rio de Janeiro. Private communication on experiments with H_2O ice irradiated with 1.7 MeV N^+ beams, 1999.

(15) Collado, V. M.; Farenzena, L. S.; Ponciano, C. R.; da Silveira, E. F.; Wien, K. *Surf. Sci.* **2004**, *569*, 149.

(16) Ziegler, J. F.; Biersack, J. P.; Littmark, U. *The Stopping and Range of Ions in Solids*; Permagon: New York, 1985. Downloaded from http://www.srim.org/.

(17) Farenzena, L.; de Barros, A. L. F.; Andrade, D. P. P.; Wien, K.; da Silveira, E. F. Manuscript in preparation.

(18) Cooper, B. H.; Tombrello, T. A. *Radiat. Eff.* **1984**, *80*, 203.

(19) Becker, O.; Knippelberg, W.; Wien, K. *Phys. Scr.* **1983**, *T6*, 117.

(20) Johnson, R. E. *Energetic Charged Particle Interactions with Atmospheres and Surfaces*; Springer Verlag: Heidelberg, 1990.

(21) Lancaster, G. M.; Honda, F.; Fukada, Y.; Rabelais, J. W. *J. Am. Chem. Soc.* **1979**, *101*, 1951.

(22) Martinez, R.; Ponciano, C. R.; Farenzena, L. S.; Iza, P.; Homem, M. G. P.; Naves de Brito, A.; Wien, K.; da Silveira, E. F. *Int. J. Mass. Spectrom.* **2006**, *253*, 112.

(23) Kobetich, E. J.; Katz, R. *Phys. Rev.* **1968**, *170*, 391–396.

(24) See, for instance, articles in Sigmund, P., Ed. *Fund. Proc. Sput. At. and Mol. (SPUT92)*; Mathematisk-fysiske meddelelser; 1985; Vol. 43, p 403.

(25) Watson, C. C.; Tombrello, T. A. *Radiat. Eff.* **1985**, *89*, 263.

(26) Liu, H. T.; Müller, J. P.; Beutler, M.; Ghotbi, M.; Noack, F.; Radloff, W.; Zhavoronkov, N.; Schulz, C. P.; Hertel, I. V. *J. Chem. Phys.* **2011**, *134*, 094305.

(27) Mihesan, C.; Ziskind, M.; Chazallon, B.; Focsa, C.; Destombes, J. L. *Appl. Surf. Sci.* **2005**, *248*, 238–242.

(28) Hedin, A.; Hakansson, P.; Salehpour, M.; Sundqvist, B. U. R. *Phys. Rev. B* **1987**, *35*, 7377.

(29) (a) Herman, V.; Kay, B. D.; Castleman, A. W. *Chem. Phys.* **1992**, *72*, 1895. (b) Radi, P. P.; Beaud, P.; Franzke, D.; Frey, H. M.; Gerber, T.; Mishcler, T.; Tzannis, A.-P. *Chem. Phys.* **1999**, *111*, 512.

(30) Wojciechowski, I. A.; Sun, S.; Szakal, C.; Winograd, N.; Garrison, B. J. *J. Phys. Chem. A* **2004**, *108*, 2993–2998.

(31) Kaneda, M.; Shimizu, M.; Hayakawa, T.; Nishimura, A.; Iriki, Y.; Tsuchida, H.; Imai, M.; Shibata, H.; Itho, A. *Nucl. Instrum. Methods Phys. Res., Sect. B* **2009**, *267/6*, 908.

(32) Kozak, R. E.; Jordan, P. C. *J. Chem. Phys.* **1993**, *99*, 2978.

(33) Matsuo, T.; Tonuma, T.; Kumagai, H.; Shibata, H.; Tawara, H. *J. Chem. Phys.* **1994**, *101*, 5356.

(34) Blake, D. F.; Jenniskens, P. *Sci. Am.* **2001**, 37.
(35) Most, M.; Wien, K.; Brunelle, A.; Della Negra, S.; Depauw, J.; Jacquet, D.; Pautrat, M.; LeBeyec, Y. *Nucl. Instrum. Methods Phys. Res., Sect. B* **2000**, *B168*, 203. **2000**, *B164*, 772.